Special odd-even effects of electron transport through quantum-dot molecules with side-coupled Majorana zero modes

Tong Gong,[1] Lian-Lian Zhang,[1] Cui Jiang,[2] Shu-Feng Zhang,[3] and Wei-Jiang Gong [1]

[1]*College of Sciences, Northeastern University, Shenyang 110819, China*
[2]*Basic Department, Shenyang Institute of Engineering, Shenyang 110136, China*
[3]*School of Physics and Technology, University of Jinan, Jinan 250022, China*

We investigate the electron transport through a serially coupled quantum-dot molecule in which each dot is side-coupled to one Majorana zero mode (MZM) at an end of the topological-superconducting nanowire. Calculation results show that with the increase of dot number, the zero-bias conductance does not display the conventional odd-even effect but always keeps equal to $\frac{e^2}{h}$. On the other hand, if different superconducting phases are added to the dot-MZM couplings with the left-right asymmetry mode, the zero-bias conductances display apparent odd-even effect. Namely, in the odd-dot cases, the zero-bias conductances are less determined by the superconducting phase, whereas they are more dependent on the superconducting phase in the cases of even dots. Regarding the shot-noise Fano factors, they also exhibit clear odd-even effects, mainly manifested as the dependence of the relation between zero-bias Fano factors and superconducting phase difference on the parity of dot number. We believe that these results are helpful to construct mesoscopic cells based on quantum dots and MZMs.

DOI: 10.1103/PhysRevResearch.5.043162

I. INTRODUCTION

In the field of condensed-matter physics, due to its ability to achieve fault-tolerant topological quantum computation in nanoscale devices, the study of Majorana topological quasiparticles has attracted wide-ranging attention [1–5]. Initially, Kitaev proposed a model in theory for this novel quasiparticle, that is, a one-dimensional (1D) *p*-wave superconductor [6,7]. Since a *p*-wave superconductor is very rare in nature [8,9], this type of quasiparticle can be induced by other methods, e.g., the semiconducting nanowire with strong Rashba spin-orbit coupling [10–15]. By applying the external magnetic field to break the time-reversal symmetry, spinless electrons with *p*-wave superconducting pairing can be effectively generated, availably realizing the 1D topological-superconducting (TS) nanowire [16]. Such a nanowire can thus be equivalent to the Kitaev model. In the past few years, following the continuous improvement of sample growth and characterization technology, more consistent experimental evidence for Majorana bound states in semiconducting wires has emerged [17–20]. Therefore, Majorana-related issues is an exciting development for researchers.

The "Majorana signatures" in these studies are characterized by the zero-bias peak in the conductance of the device, which is due to the robust zero-energy mode at the edges of the wire. In such a case, this unique signature is the so-called Majorana zero mode (MZM). However, besides MZMs,

other physical mechanisms can also form the zero-bias conductance peaks, such as the Kondo effect [21,22] and the formation of zero-energy Andreev bound states [23–28]. As a result, how to distinguish MZMs from other phenomena is very important. So far, large quantities of ideas have been put forward [20,29–32], for instance, observing the degree of Majorana nonlocality [20,30] and measuring the signature of non-Abelian statistics [4]. Although such features are crucial to the realization of fault-tolerant quantum computation, their measurements are always difficult.

According to current research progress, a universal way for detecting MZMs is to attach quantum dots (QDs) to the end of a topological-superconducting nanowire. The signature of MZM can be determined by measuring the conductance through QDs [33–35]. It can be observed that the MZM at the end of the nanowire "leaks" into the attached QD. For the single-QD case, the zero-bias conductance is found to be halved to $\frac{e^2}{2h}$ [33]. Such a result has also been observed in the T-shaped multiple-QD structure [36]. Alternatively, in the double-QD structure, the leakage effect enables to result in a half-suppression of the second stage of the Kondo effect, which is revealed through fractional values of the charge conductances [37]. Compared with other methods, it has an obvious advantage in that there is no direct charge transfer between MZM and QD, thus preventing quasiparticle "poisoning" [38]. In recent years, QD-assisted topological structures have been realized in some experiments [19,20], which provides strong evidence for the detection of MZM using QDs.

In addition to the detection of MZMs, one can find further characteristics of MZMs by changing the relevant parameters of QDs. In this paper we consider a QD molecule in which the serially coupled QDs are side-coupled to MZMs at the
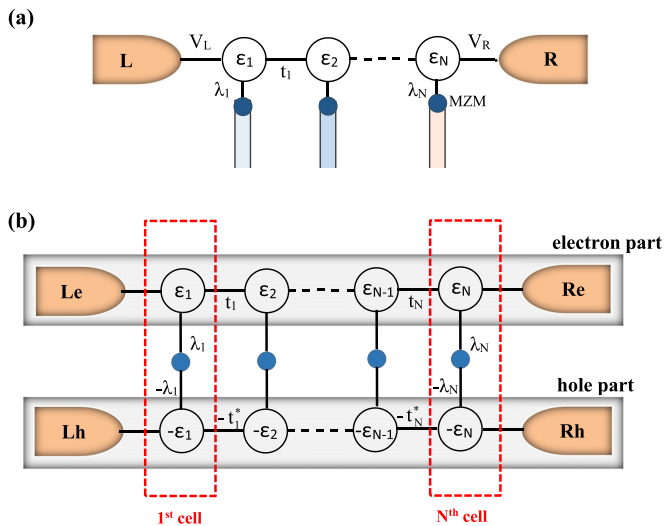
(a)

(b)

FIG. 1. (a) Schematic of the QD molecule with side-coupled MZMs. MZMs are generated at the two ends of TS nanowires, and each MZM is coupled to one QD in the serially coupled QD molecule, respectively. (b) Schematics of our considered structure in the Nambu representation.

ends of TS nanowires [see Fig. 1(a)]. Our purpose is to clarify the conductance properties in this geometry. After calculation, we observe that in this structure with $N > 1$ (N is the QD number), the zero-bias conductance does not display the odd-even effect of the MZM-absent case, whereas it is always equal to $\frac{e^2}{h}$. Such a result is completely different from the case without MZMs. Instead, when superconducting phase differences are taken into account, the zero-bias conductances will display alternative interesting phenomena which are also related to the parity of the QD number. All these results suggest the various interplay manners between the electron tunneling (ET) and local Andreev reflection (LAR). These results are helpful to integrate the mesoscopic cells based on QDs and MZMs.

The paper is structured as follows. In Sec. II we introduce the model of the multiple QD-MZM structure. Then we deduce current formulas to investigate the transport behaviors using the scattering-matrix method, which is combined with the nonequilibrium Green's function technique. In Sec. III we present the numerical results of conductances and Fano factors, accompanied by a detailed explanation about them. Then we summarize the leading results of this work in Sec. IV. Finally, we give some detailed calculations in Appendixes A, B, and C.

II. THE THEORETICAL MODEL

Our considered QD molecule is illustrated in Fig. 1(a). As shown in this figure, such a molecule is formed by the serially coupling of the QDs. Each QD in the main channel is coupled to one MZM in the corresponding TS nanowire. The Hamiltonian for our considered system is written as

$$H = H_C + H_{MD} + H_V. \tag{1}$$

In Eq. (1) the first term is the Hamiltonian for the two normal metallic leads. It takes the form as

$$H_C = \sum_{\alpha k} \varepsilon_{\alpha k} c_{\alpha k}^\dagger c_{\alpha k}, \tag{2}$$

where $c_{\alpha k}^\dagger$ ($c_{\alpha k}$) is an operator to create (annihilate) an electron of the continuous state $|k\rangle$ in lead α ($\alpha \in L, R$), and $\varepsilon_{\alpha k}$ is the corresponding energy of state $|k\rangle$. The second term is the Hamiltonian of the QDs and their coupling to MZMs, which is written as $H_{MD} = \sum_{j=1}^{N} \mathcal{H}_{md} + \mathcal{H}_t$, with

$$\mathcal{H}_{md} = \varepsilon_j d_j^\dagger d_j + i\zeta_j \eta_{j1}\eta_{j2} + (\lambda_j^* d_j^\dagger - \lambda_j d_j)\eta_{j1}$$

and

$$\mathcal{H}_t = \sum_{j}^{N-1} t_j d_{j+1}^\dagger d_j + \text{H.c.}, \tag{3}$$

where $d_j^\dagger$ (d_j) is the creation (annihilation) operator in QD-j, and ε_j is the corresponding level. Here the Coulomb interaction in the QD is ignored, since we are mainly interested in the interplay between the electronic bound state and MZMs. The second term in Eq. (3) describes the low-energy effective Hamiltonian for the MZMs in the jth TS nanowire, where η_{jn} ($n = 1, 2$) is the self-Hermitian operator for the nth MZM with $\eta_{jn} = \eta_{jn}^\dagger$. ζ_j denotes the inter-MZM coupling in the jth TS nanowire. In this work we would like to take $\zeta_j = 0$, since we are interested in the case of MZM. λ_j is the coupling coefficient between the jth MZM and the corresponding QD [32]. In addition, t_j denotes the interdot coupling coefficient in the main channel. Next, the last term in Eq. (1) represents the QD-lead coupling. Its explicit form can be expressed as

$$H_V = \sum_{\alpha k} V_L c_{Lk}^\dagger d_1 + \sum_{\alpha k} V_R c_{Rk}^\dagger d_N + \text{H.c.}, \tag{4}$$

where V_α describes the QD-lead coupling coefficient.

To evaluate the electron transport properties through our considered system, i.e., the current, we would like to use the scattering-matrix approach, which also allows for AR processes [39,40]. This yields the current

$$I_\alpha = \frac{e}{h} \int d\epsilon \sum_x \text{sgn}(x) \sum_{\beta;y} A_{\beta,\beta;y,y}^{(\alpha x)} n_{\beta,x}, \tag{5}$$

where Greek indices denote electron (e) and hole (h) channels with $\text{sgn}(e) = +1$ and $\text{sgn}(h) = -1$, and

$$A_{\beta,\gamma;y,z}^{(\alpha x)} = \delta_{\alpha\beta}\delta_{\alpha\gamma}\delta_{xy}\delta_{xz} - s_{\alpha,\beta}^{xy*} s_{\alpha,\gamma}^{xz}. \tag{6}$$

The reservoir distribution functions $n_{k,\gamma}$ are Fermi functions with different chemical potentials for the electron and hole bands $n_{\beta,x}^{-1} = 1 + \exp\{[\epsilon - \text{sgn}(x)\mu_\beta]/(k_B T)\}$ (where k_B is the Boltzmann constant and T denotes temperature). The coefficients $s_{\alpha,\beta}^{xy}$ are the elements of the S matrix,

$$S(\omega) = 1 - 2\pi i \mathbf{W}^\dagger \mathbf{G}^r \mathbf{W}, \tag{7}$$

where $\mathbf{W}$ describes the coupling between the states of the system without leads and the scattering states in the leads, and $\mathbf{G}^r = [\epsilon(\mathbf{I}_D + \frac{1}{2}\mathbf{I}_M) - H_{MD} + i\pi \mathbf{WW}^\dagger]^{-1}$ is the retarded Green function for the system with self-energy $i\pi \mathbf{WW}^\dagger$. The coupling matrix $\mathbf{W}$ in the lead basis $\{\psi_L^\dagger, \psi_R^\dagger, \psi_L, \psi_R\}$ is given

by $[\mathbf{W}]_{jl} = \text{sgn}(\alpha)\sqrt{\Gamma_\alpha/2}\,\delta_{jl}$, where $\Gamma_\alpha = 2\pi|V_\alpha|^2\rho_\alpha$ denotes the coupling strength between QD-1(N) and lead $L(R)$. Here, $\mathbf{I}_D$ ($\mathbf{I}_M$) represent the identity matrix in the QD (Majorana) space. Meanwhile, the matrix form of the Green function can be written out, i.e.,

$$[\mathbf{G}^r]^{-1} = \begin{bmatrix} \mathbf{g}_1^{-1} & -\mathcal{H}_{t1} & 0 & \cdots & 0 \\ -\mathcal{H}_{t1}^\dagger & \mathbf{g}_2^{-1} & -\mathcal{H}_{t2} & 0 & \vdots \\ 0 & \cdots & \ddots & \cdots & 0 \\ \vdots & \cdots & -\mathcal{H}_{t,N-2}^\dagger & \mathbf{g}_{N-1}^{-1} & -\mathcal{H}_{t,N-1} \\ 0 & \cdots & 0 & -\mathcal{H}_{t,N-1}^\dagger & \mathbf{g}_N^{-1} \end{bmatrix},$$

$$(8)$$

with

$$[\mathbf{g}_j]^{-1} = \begin{bmatrix} g_{je}^{-1} & -\lambda_j^* & 0 \\ -\lambda_j & z & \lambda_j^* \\ 0 & \lambda_j & g_{jh}^{-1} \end{bmatrix}$$

$$(9)$$

and

$$\mathcal{H}_{tj} = \begin{bmatrix} t_j^* & 0 & 0 \\ 0 & 0 & 0 \\ 0 & 0 & -t_j \end{bmatrix}.$$

$$(10)$$

In the above equations, $z = \epsilon + i0^+$ and $g_{je(h)}(z) = [z \mp \varepsilon_j + i\Gamma(\delta_{j1} + \delta_{jN})]^{-1}$ is the zero-order Green function of the QDs unperturbed by MZMs, in which $\Gamma = \frac{1}{2}(\Gamma_L + \Gamma_R)$.

From Eq. (5), respective components of I_L can be well defined (*by using the relationship that* $\sum_{y,\beta}|s_{\alpha,\beta}^{xy}(\omega)|^2 = 1$): $I_L = I_L^{ET} + I_L^{LAR} + I_L^{CAR}$, where

$$I_L^{ET} = \frac{e}{h}\int d\epsilon\, T_{L,R}^{ee}(\epsilon)[n_{L,e}(\epsilon) - n_{R,e}(\epsilon)], \quad (11)$$

$$I_L^{LAR} = \frac{e}{h}\int d\epsilon\, T_{L,L}^{eh}(\epsilon)[n_{L,e}(\epsilon) - n_{L,h}(\epsilon)], \quad (12)$$

$$I_L^{CAR} = \frac{e}{h}\int d\epsilon\, T_{L,R}^{eh}(\epsilon)[n_{L,e}(\epsilon) - n_{R,h}(\epsilon)], \quad (13)$$

with $T_{\alpha,\beta}^{xy}(\epsilon) = |s_{\alpha,\beta}^{xy}(\epsilon)|^2$. To be concrete,

$$\begin{aligned} T_{L,R}^{ee}(\epsilon) &= \left|s_{L,R}^{ee}(\epsilon)\right|^2 = \Gamma_L\Gamma_R\left|G_{1e,Ne}^r(\epsilon)\right|^2, \\ T_{L,L}^{eh}(\epsilon) &= \left|s_{L,L}^{eh}(\epsilon)\right|^2 = \Gamma_L\Gamma_L\left|G_{1e,1h}^r(\epsilon)\right|^2, \\ T_{L,R}^{eh}(\epsilon) &= \left|s_{L,R}^{eh}(\epsilon)\right|^2 = \Gamma_L\Gamma_R\left|G_{1e,Nh}^r(\epsilon)\right|^2. \end{aligned} \quad (14)$$

They describe the currents of ET, LAR, and crossed Andreev reflection, respectively. In this work we would like to take $\mu_L = \frac{eV_b}{2}$ and $\mu_R = -\frac{eV_b}{2}$ (where μ_α is the chemical potential of lead α), and then the difference between μ_L and μ_R will drive the ET and LAR processes. In lead L, the current formula can be written as [36]

$$I_L = \frac{e}{h}\int d\epsilon\left[T_{L,R}^{ee}(\epsilon)(n_{L,e} - n_{R,e}) + T_{L,L}^{eh}(\epsilon)(n_{L,e} - n_{L,h})\right]. \quad (15)$$

Since we are only interested in the zero-temperature case, our structure obeys the relationship that $n_{L,e}(\epsilon) = 1 - n_{R,e}(-\epsilon)$.

Therefore there exists $n_{R,e} = n_{L,h}$ in our system, and then the above current formula can be simplified as

$$I = \frac{e}{h}\int d\epsilon\, \mathcal{T}(\epsilon)(n_{L,e} - n_{R,e}), \quad (16)$$

with $\mathcal{T}(\epsilon) = T_{L,R}^{ee}(\epsilon) + T_{L,L}^{eh}(\epsilon)$.

In comparison with the current properties, the conductance is more effective to describe the transport properties because it is related to transmission ability directly. At the zero-temperature limit, the differential conductance is given as

$$\mathbb{G} = \frac{e^2}{2h}\left[\mathcal{T}\left(\epsilon = \frac{eV_b}{2}\right) + \mathcal{T}\left(\epsilon = -\frac{eV_b}{2}\right)\right]. \quad (17)$$

As a typical case of zero-bias voltage, the conductance can be simplified as $\mathbb{G} = \frac{e^2}{h}\mathcal{T}(V_b = 0)$ [41,42], with its LAR and ET components defined as $\mathbb{G}_{V_b=0}^{LAR} = \frac{e^2}{h}\mathcal{T}_{L,L}^{eh}(\epsilon = 0)$ and $\mathbb{G}_{V_b=0}^{ET} = \frac{e^2}{h}\mathcal{T}_{L,R}^{ee}(\epsilon = 0)$, respectively. Therefore the transport properties in this system can be clarified by studying the LAR and ET characteristics.

III. NUMERICAL RESULTS AND DISCUSSION

Following the formulations developed in the above section, we continue to perform numerical calculations to investigate the electron transport through our considered QD-molecule structure. In the context, the system temperature is taken to be zero. The interdot couplings are supposed to be uniform with $t_j = t = 0.5$, and the lead-QD coupling is considered to be $\Gamma_\alpha = \Gamma = 0.5$. The unit of these parameters can be supposed as 10^{-1} meV according to the relevant experiments [43]. In addition, we would like to take λ_1 to be real with $\lambda_1 = |\lambda_1|$ for calculation.

It is known that for the conventional serially coupled QDs with $\varepsilon_j = 0$, the zero-bias conductance displays apparent odd-even effect with the enlargement of the QD molecule. Namely, for the case of odd-number QDs, the zero-bias conductance shows up as a resonant peak, whereas it only exhibits a conductance dip for the case of even-number QDs [44,45]. The detailed conductance expressions are given as

$$\mathbb{G}_{V_b=0} = \frac{e^2}{h}\frac{-8\Gamma_L|t_1|^2\,\text{Im}\,G_{2N}^r}{\left(\Gamma_L - 2|t_1|^2\,\text{Im}\,G_{2N}^r\right)^2}, \quad (18)$$

where

$$\text{Im}\,G_{2N}^r = -\frac{\Gamma_R}{2}\left|\frac{t_3 t_5 \cdots t_{N-2}}{t_2 t_4 \cdots t_{N-1}}\right|^2, \quad N \in \text{odd};$$

$$\text{Im}\,G_{2N}^r = -\frac{2}{\Gamma_R}\left|\frac{t_3 t_5 \cdots t_{N-1}}{t_2 t_4 \cdots t_{N-2}}\right|^2, \quad N \in \text{even}.$$

Accordingly, in the case of $t_j = t$ and $\Gamma_\alpha = \Gamma$, $\mathbb{G}_{V_b=0} = \frac{e^2}{h}$ ($N \in$ odd) and $\mathbb{G}_{V_b=0} = \frac{e^2}{h}\frac{16\Gamma^2 t^2}{(\Gamma^2 + 4t^2)^2}$ ($N \in$ even).

Meanwhile, we would like to review the simplest case of our structure with $N = 1$, though it has been discussed in Refs. [33,36]. In such a case, the Green functions for the LAR
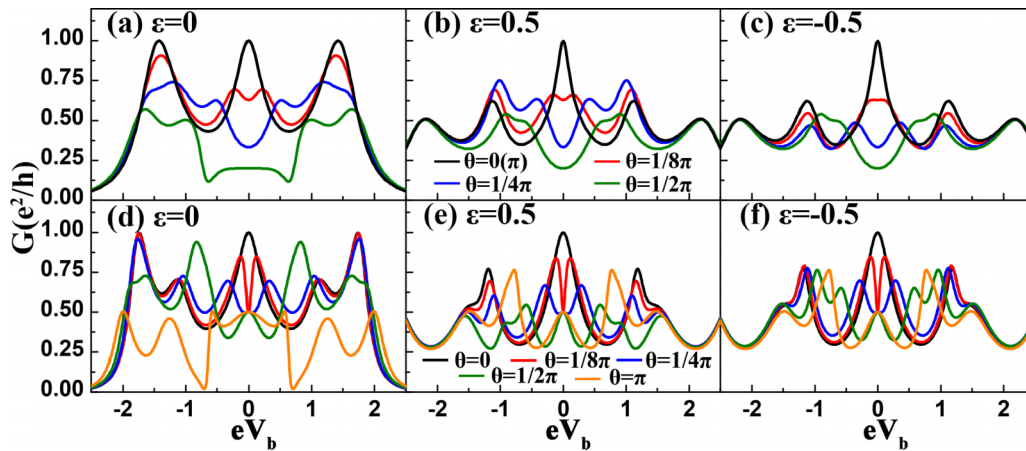
FIG. 2. Spectra of differential conductance in the configurations of $N = 2$ and $N = 3$, with the increase of the inter-MZM phase difference. The QD-MZM couplings are assumed to be identical with $|\lambda_j| = \lambda_0 = 0.4$. (a)–(c) The conductance of $N = 2$, in the case of $\varepsilon = 0$ and ± 0.5, respectively. (d)–(f) Corresponding results of $N = 3$.

and ET processes are given as

$$
G^r_{1e,1h} = \frac{-|\lambda_1|^2}{\epsilon(\epsilon - \varepsilon_1 + i\Gamma)(\epsilon + \varepsilon_1 + i\Gamma) - 2|\lambda_1|^2(\epsilon + i\Gamma)},
$$

$$
G^r_{1e,1e} = \frac{\epsilon(\epsilon + \varepsilon_1 + i\Gamma) - |\lambda_1|^2}{\epsilon(\epsilon - \varepsilon_1 + i\Gamma)(\epsilon + \varepsilon_1 + i\Gamma) - 2|\lambda_1|^2(\epsilon + i\Gamma)}.
$$

(19)

Thus at the limit of $\epsilon \to 0$, $G^r_{1e,1h}|_{\epsilon \to 0} = G^r_{1e,1e}|_{\epsilon \to 0} = \frac{1}{2i\Gamma}$. With the help of Eq. (14), we are allowed to present the zero-bias conductance, i.e., $\mathbb{G}_{V_b=0}(N=1) = 2\mathbb{G}^{\mathrm{LAR(ET)}}_{V_b=0}$ $(N=1) = \frac{e^2}{2h}$. Such a result exactly describes the leakage effect.

Following the single-QD result, we would like to enlarge the size of the QD molecule to investigate the variation properties of the differential conductance. Our purpose is to clarify the change of the odd-even effect of the zero-bias conductance due to the side coupling of the MZMs, as well as the characteristics of the leakage effect. To begin with, we consider the cases of $N = 2$ and $N = 3$, respectively. Note that in these cases, the QD-MZM couplings are allowed to different superconducting phases caused by the respective TS nanowires. We thus perform calculation about the case of $N = 2$ by considering $\lambda_1 = \lambda_0 e^{i\theta/2}$ and $\lambda_2 = \lambda_0 e^{-i\theta/2}$, with θ being the superconducting phase difference. For the case of $N = 3$, we take the left-right asymmetric superconducting phase (ASP) mode where $\lambda_1 = \lambda_0 e^{i\theta/2}$, $\lambda_2 = \lambda_0$, and $\lambda_3 = \lambda_0 e^{-i\theta/2}$. Regarding the QD levels, we take $\varepsilon_j = \varepsilon$. The differential conductance spectra are shown in Fig. 2. Figures 2(a)–2(c) display the results of $N = 2$, with $\varepsilon = 0$ and ± 0.5, respectively. In Fig. 2(a) where $\varepsilon = 0$, it can be found that at $\theta = 0$, three resonant peaks appear in the differential conductance spectrum. The underlying reason lies in the twofold degeneracy of the eigenstates, because in such a case $E_{1(2)} = -\sqrt{2\lambda_0^2 + t_1^2} = -E_{5(6)}$ and $E_{3(4)} = 0$. With the increase of θ, the conductance peaks decrease and splits. When $\theta = \frac{\pi}{2}$, one conductance plateau is formed at the low-bias region with its magnitude about being $\frac{0.2e^2}{h}$. However, the further increase of θ will enhance the conductance magnitude. To be concrete,

when $\theta = \pi$, the conductance profile is consistent with the result of $\theta = 0$. This means that with the change of superconducting phase difference, the conductance varies in period π. Next, as the QD levels depart from zero, e.g., $\varepsilon = \pm 0.5$, only the resonant peak at the zero-bias limit survives in the conductance spectrum, in comparison with the result of $\varepsilon = 0$. Although the conductance spectra of $\varepsilon = \pm 0.5$ exhibit a little difference, they show the similar change manner with the increase of θ. Also, in the case of $\theta = \pi$, the conductances become consistent with those of $\theta = 0$. These results indicate that for the double-QD molecule, the side-coupling of MZMs can enhance the zero-bias conductance. Also, the conductance spectra can be modified in a substantial way following the change of superconducting phase difference.

The conductance results of $N = 3$ are shown in Figs. 2(d)– 2(f). One can find that the variation manners of the conductance spectra are basically similar to the case of $N = 2$, following the shift of QD levels. Namely, at $\varepsilon = 0$, three resonant peaks arise in the conductance spectra with their values close to $\frac{e^2}{h}$, despite the appearance of subpeaks. Following their departure from the energy zero point, the nonzero-bias peaks are suppressed. Besides, with the change of θ, the conductance peaks are suppressed gradually in this progress, accompanied by the further oscillation of the conductance curves. On the other hand, in this case, at the zero-bias limit, the conductance variation is different from the case of $N = 2$. One can find that at the case of $\theta = 0$, the conductance reaches its maximum with $\mathbb{G}(eV_b = 0) = \frac{e^2}{h}$. Once the superconducting phase difference is introduced, the conductance magnitude is halved. The further increase of θ cannot change this conductance value, including $\theta = \pi$. Therefore the leakage effect of the MZMs, characterized by the zero-bias conductance, displays the two-stage results with the change of the superconducting phase difference, which is also different from the case of $N = 2$.

In order to explain the conductance results, we would like to present the analytical expression of the zero-bias conductance with the help of the Green functions in Appendixes A and B. At the limit of $\epsilon \to 0$, we can obtain the

results that under the condition of complex λ_j, if $N = odd$ $(N > 1)$,

$$G^r_{1e,1h}|_{\epsilon \to 0} = \frac{1}{\Lambda_N} \lambda_1^2 |t_2|^2 (\lambda_2^* \lambda_3 - \lambda_2 \lambda_3^*)^2 \cdots$$
$$\times |t_{N-1}|^2 (\lambda_{N-1}^* \lambda_N - \lambda_{N-1} \lambda_N^*)^2, \quad (20)$$

with $\Lambda_N = i\Gamma_L |\lambda_1 t_2|^2 (\lambda_2^* \lambda_3 - \lambda_2 \lambda_3^*)^2 \cdots |t_{N-1}|^2 (\lambda_{N-1}^* \lambda_N - \lambda_{N-1} \lambda_N^*)^2 + i\Gamma_R |t_1|^2 (\lambda_1^* \lambda_2 - \lambda_1 \lambda_2^*)^2 \cdots |t_{N-2}|^2 (\lambda_{N-2}^* \lambda_{N-1} - \lambda_{N-2} \lambda_{N-1}^*)^2 |\lambda_N|^2$. If $N = even$,

$$G^r_{1e,1h}|_{\epsilon \to 0} = \frac{i\Gamma_R}{\Lambda_N} \lambda_1^2 |t_2|^2 (\lambda_2^* \lambda_3 - \lambda_2 \lambda_3^*)^2 \cdots$$
$$\times (\lambda_{N-1}^* \lambda_N - \lambda_{N-1} \lambda_N^*)^2 |\lambda_N|^2, \quad (21)$$

with $\Lambda_N = -\Gamma_L \Gamma_R |\lambda_1 t_2|^2 (\lambda_2^* \lambda_3 - \lambda_2 \lambda_3^*)^2 \cdots |t_{N-2}|^2 (\lambda_{N-1}^* \lambda_N - \lambda_{N-1} \lambda_N^*)^2 |\lambda_N|^2 + |t_1|^2 (\lambda_1^* \lambda_2 - \lambda_1 \lambda_2^*)^2 \cdots |t_{N-1}|^2 (\lambda_{N-1}^* \lambda_N - \lambda_{N-1} \lambda_N^*)^2$. Meanwhile,

$$G^r_{1e,Ne}|_{\epsilon \to 0} = \frac{\lambda_1 \lambda_N^* t_1^* \cdots t_{N-1}^*}{\Lambda_N} (\lambda_1^* \lambda_2 - \lambda_1 \lambda_2^*)(\lambda_2^* \lambda_3 - \lambda_2 \lambda_3^*) \cdots$$
$$\times (\lambda_{N-1}^* \lambda_N - \lambda_{N-1} \lambda_N^*). \quad (22)$$

Based on these results, we know that in such a multiple QD-MZM system, the zero-energy Green functions are determined by the leakage effect of the MZMs. Moreover, we can write out the expressions of the zero-bias conductance. For the case of $N = 2$, the zero-bias conductance can be expressed explicitly, i.e., $\mathbb{G}_{V_b=0}(N = 2) = \mathbb{G}^{\mathrm{LAR}}_{V_b=0}(N = 2) + \mathbb{G}^{ET}_{V_b=0}$

$(N = 2)$, with

$$\mathbb{G}^{\mathrm{LAR}}_{V_b=0} = \frac{e^2}{h} \frac{\Gamma_L^2 \Gamma_R^2 |\lambda_1 \lambda_2|^4}{||\Gamma_L \Gamma_R |\lambda_1 \lambda_2|^2 - |t_1|^2 (\lambda_1^* \lambda_2 - \lambda_1 \lambda_2^*)^2|^2},$$

$$\mathbb{G}^{ET}_{V_b=0} = \frac{e^2}{h} \frac{\Gamma_L \Gamma_R |t_1^* \lambda_1 \lambda_2^* (\lambda_1^* \lambda_2 - \lambda_1 \lambda_2^*)|^2}{||\Gamma_L \Gamma_R |\lambda_1 \lambda_2|^2 - |t_1|^2 (\lambda_1^* \lambda_2 - \lambda_1 \lambda_2^*)^2|^2}.$$
$$[\mathbf{N = 2}] \quad (23)$$

As a typical case where $\lambda_1 = \lambda_0 e^{i\theta/2}$, $\lambda_2 = \lambda_0 e^{-i\theta/2}$, and $\Gamma_\alpha = \Gamma$, the conductance expressions can be further simplified, i.e.,

$$\mathbb{G}^{\mathrm{LAR}}_{V_b=0} = \frac{e^2}{h} \frac{\Gamma^4}{(\Gamma^2 + 4|t_1|^2 \sin^2 \theta)^2},$$

$$\mathbb{G}^{ET}_{V_b=0} = \frac{e^2}{h} \frac{4\Gamma^2 |t_1|^2 \sin^2 \theta}{(\Gamma^2 + 4|t_1|^2 \sin^2 \theta)^2}.$$
$$[\mathbf{N = 2}] \quad (24)$$

It is not difficult to find that at the case of $\theta = n\pi$, there will be $\mathbb{G}^{\mathrm{LAR}}_{V_b=0} = \frac{e^2}{h}$ and $\mathbb{G}^{ET}_{V_b=0} = 0$. This exactly means that in this case, the ET process is forbidden, whereas only the AR survives. Interpretively, destructive interference occurs in the ET process due to the side coupling of MZMs, accompanied by the constructive interference in the LAR process.

Next, in the structure of $N = 3$, we have the following zero-bias conductance results:

$$\mathbb{G}^{\mathrm{LAR}}_{V_b=0} = \frac{e^2}{h} \frac{\Gamma_L^2 |\lambda_1 t_2|^4 |\lambda_2^* \lambda_3 - \lambda_2 \lambda_3^*|^4}{|\Gamma_L |\lambda_1 t_2|^2 (\lambda_2^* \lambda_3 - \lambda_2 \lambda_3^*)^2 + \Gamma_R |\lambda_3 t_1|^2 (\lambda_1^* \lambda_2 - \lambda_1 \lambda_2^*)^2|^2},$$

$$\mathbb{G}^{ET}_{V_b=0} = \frac{e^2}{h} \frac{\Gamma_L \Gamma_R |\lambda_1 \lambda_3 t_1 t_2|^2 |(\lambda_1^* \lambda_2 - \lambda_1 \lambda_2^*)(\lambda_2^* \lambda_3 - \lambda_2 \lambda_3^*)|^2}{|\Gamma_L |\lambda_1 t_2|^2 (\lambda_2^* \lambda_3 - \lambda_2 \lambda_3^*)^2 + \Gamma_R |\lambda_3 t_1|^2 (\lambda_1^* \lambda_2 - \lambda_1 \lambda_2^*)^2|^2}.$$
$$[\mathbf{N = 3}] \quad (25)$$

If $\lambda_2^* \lambda_3 - \lambda_2 \lambda_3^* = \pm(\lambda_1^* \lambda_2 - \lambda_1 \lambda_2^*) \neq 0$, there will be

$$\mathbb{G}^{\mathrm{LAR}}_{V_b=0} = \frac{e^2}{h} \frac{\Gamma_L^2 |\lambda_1 t_2|^4}{||\Gamma_L |\lambda_1 t_2|^2 + \Gamma_R |\lambda_3 t_1|^2|^2},$$

$$\mathbb{G}^{ET}_{V_b=0} = \frac{e^2}{h} \frac{\Gamma_L \Gamma_R |\lambda_1 \lambda_3 t_1 t_2|^2}{||\Gamma_L |\lambda_1 t_2|^2 + \Gamma_R |\lambda_3 t_1|^2|^2}.$$
$$[\mathbf{N = 3}] \quad (26)$$

In Figs. 2(d)–2(f), the coupling coefficients between the MZMs and the corresponding QDs are taken to be the left-right ASP mode with $\lambda_1 = \lambda_0 e^{i\theta/2}$, $\lambda_2 = \lambda_0$, and $\lambda_3 = \lambda_0 e^{-i\theta/2}$, and then in the case of $t_j = t$, the zero-bias conductance expressions can be further simplified, i.e.,

$$\mathbb{G}^{\mathrm{LAR}}_{V_b=0} = \frac{e^2}{h} \frac{\Gamma_L^2}{(\Gamma_L + \Gamma_R)^2},$$

$$\mathbb{G}^{ET}_{V_b=0} = \frac{e^2}{h} \frac{\Gamma_L \Gamma_R}{(\Gamma_L + \Gamma_R)^2}. \quad (27)$$

Under the condition of $\Gamma_\alpha = \Gamma$, we can find that $\mathbb{G}^{\mathrm{LAR}}_{V_b=0} = \mathbb{G}^{ET}_{V_b=0} = \frac{e^2}{4h}$, leading to the result of $\mathbb{G}_{V_b=0} = \frac{e^2}{2h}$.

Alternatively, if $\lambda_1 \lambda_2^*$ is real, we will obtain the other result, i.e., $\mathbb{G}^{\mathrm{LAR}}_{V_b=0} = \frac{e^2}{h}$ and $\mathbb{G}^{ET}_{V_b=0} = 0$, since only the LAR process is allowed, as shown in Eq. (A13). All these analytical results suggest the abundant conductance properties induced by the respective QD-MZM couplings.

We anticipate that in this multiple QD-MZM structure without superconducting phase difference, the zero-bias conductances do not display any odd-even effect but always keep equal to $\frac{e^2}{h}$. On the other hand, in the presence of a finite superconducting phase difference among MZMs, the zero-bias conductance is allowed to the odd-even effect, manifested as the halved conductance peak in the structures with odd QDs. Following this understanding, in Fig. 3 we would like to present the differential conductance spectra in the structure of $N = 4$ by increasing the superconducting phase difference. Due to the complication of this structure, we would like to pay attention to two typical cases with left-right ASP mode, i.e., $\lambda_{1(2)} = \lambda_{3(4)}^* = \lambda_0 e^{i\theta/2}$ and $\lambda_1 = \lambda_4^* = \lambda_0 e^{i\theta/2}$, with $\lambda_2 = \lambda_3^* = \lambda_0 e^{i\theta/6}$. Note that such an assumption also guarantees the identical phase difference between λ_1 and λ_N. For the former case, in Figs. 3(a)–3(c) we see that at $\varepsilon = 0$, the
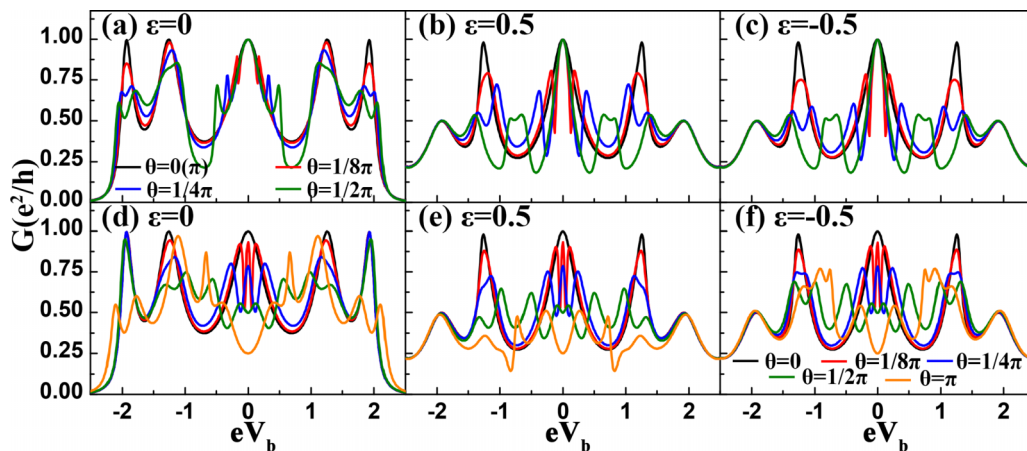
FIG. 3. Spectra of differential conductance in the configurations of $N = 4$ with the increase of the inter-MBS phase difference. The QD-MBS couplings are assumed to be identical with $|\lambda_j| = \lambda_0 = 0.4$. (a)–(c) The conductance of $\lambda_{1(2)} = \lambda_0 e^{i\theta/2} = \lambda_{3(4)}^*$, in the cases of $\varepsilon = 0$ and ± 0.5, respectively. (d)–(f) Corresponding results of $\lambda_1 = \lambda_4 = \lambda_0 e^{i\theta/2}$ and $\lambda_2 = \lambda_3^* = \lambda_0 e^{i\theta/6}$.

conductance spectrum displays the profile with five resonant peaks in the absence of superconducting phase difference. When the superconducting phase difference is introduced, the nonzero-bias peaks decrease and split, leading to the further oscillation of the conductance curve. Meanwhile, new sub-peaks appear around the zero-bias peaks. Next for $\varepsilon = \pm 0.5$, the conductance spectra show the same profiles. In the absence of a superconducting phase difference, three resonant peaks survive in the conductance spectra, with the suppression of the two peaks at high- and low-bias limits. Regarding the effect of θ, it is to induce the decrease of nonzero-bias conductance peaks. We then consider that in this case, the switch effect of the superconducting phase difference is relatively weak. On the other hand, for the latter case, in Figs. 3(d)–3(f) one can find the distinct results. In the case

of $\varepsilon = 0$, increasing the superconducting phase difference modifies the oscillation of the conductance curve seriously, accompanied by the peak-to-valley transition of the zero-bias conductance. Next, in the case of $\varepsilon = \pm 0.5$, the leading conductance changes are similar to those in Figs. 3(b) and 3(c), but the zero-bias conductance is consistent with the result in Fig. 3(d). According to these results, we know that in the structure of $N = 4$, the zero-bias conductance displays different variation manners when the superconducting phase difference is applied partly or fully to the QD-MZM coupling coefficients.

Similar to the cases of $N = 2$ and $N = 3$, we would like to present the derivation results in the structure of $N = 4$ to clarify the influence of structural parameters. Accordingly, the zero-bias conductance can be given as

$$
\mathbb{G}^{\mathrm{LAR}}_{V_b=0} = \frac{e^2}{h} \frac{\Gamma_L^2 \Gamma_R^2 |\lambda_1 \lambda_4 t_2|^4 |\lambda_2^* \lambda_3 - \lambda_2 \lambda_3^*|^4}{|\Gamma_L \Gamma_R |\lambda_1 \lambda_4 t_2|^2 (\lambda_2^* \lambda_3 - \lambda_2 \lambda_3^*)^2 - |t_1 t_3|^2 (\lambda_1^* \lambda_2 - \lambda_1 \lambda_2^*)^2 (\lambda_3^* \lambda_4 - \lambda_3 \lambda_4^*)^2|^2},
$$

$$
\mathbb{G}^{ET}_{V_b=0} = \frac{e^2}{h} \frac{\Gamma_L \Gamma_R |\lambda_1 \lambda_4 t_1 t_2 t_3|^2 |(\lambda_1^* \lambda_2 - \lambda_1 \lambda_2^*)(\lambda_2^* \lambda_3 - \lambda_2 \lambda_3^*)(\lambda_3^* \lambda_4 - \lambda_3 \lambda_4^*)|^2}{|\Gamma_L \Gamma_R |\lambda_1 \lambda_4 t_2|^2 (\lambda_2^* \lambda_3 - \lambda_2 \lambda_3^*)^2 - |t_1 t_3|^2 (\lambda_1^* \lambda_2 - \lambda_1 \lambda_2^*)^2 (\lambda_3^* \lambda_4 - \lambda_3 \lambda_4^*)^2|^2}.
$$

$$[\mathbf{N = 4}] \tag{28}$$

As a matter of fact, these formulas show that when the superconducting phase difference is partly applied, e.g., $\lambda_{1(2)} = \lambda_{3(4)}^* = \lambda_0 e^{i\theta/2}$, there will be $\mathbb{G}^{\mathrm{LAR}}_{V_b=0} = \frac{e^2}{h}$ and $\mathbb{G}^{ET}_{V_b=0} = 0$. Such a result is identical with that of the zero superconducting phase difference [see Eq. (A13)]. For the other type of superconducting phase difference, i.e., $\lambda_1 = \lambda_4^* = \lambda_0 e^{i\theta/2}$ with $\lambda_2 = \lambda_3^* = \lambda_0 e^{i\theta/6}$, there will be

$$
\mathbb{G}^{\mathrm{LAR}}_{V_b=0} = \frac{e^2}{h} \frac{\Gamma^4}{\left(\Gamma^2 + 4t^2 \sin^2 \frac{\theta}{3}\right)^2},
$$

$$
\mathbb{G}^{ET}_{V_b=0} = \frac{e^2}{h} \frac{4\Gamma^2 t^2 \sin^2 \frac{\theta}{3}}{\left(\Gamma^2 + 4t^2 \sin^2 \frac{\theta}{3}\right)^2},
$$

$$[\mathbf{N = 4}] \tag{29}$$

under the condition of $\Gamma_\alpha = \Gamma$ and $t_j = t$. Such a result is formally the same as the double-QD case. As a matter of fact, one can find that when superconducting phase difference is partly applied in other manners, e.g., $\lambda_1 = \lambda_{2(3,4)}^* = \lambda_0 e^{i\theta/2}$, or $\lambda_1 = \lambda_{3(4)}^* = \lambda_0 e^{i\theta}$ with $\lambda_2 = \lambda_0$, the result of $\lambda_{2j-1}\lambda_{2j}^*$ will stay real, and then $\mathbb{G}^{\mathrm{LAR}}_{V_b=0} = \frac{e^2}{h}$ and $\mathbb{G}^{ET}_{V_b=0} = 0$ can still be observed. So far, from the results of $N = 1$ to $N = 4$, we have gotten the further understanding that when the QD-MZM couplings carry different superconducting phases, our QD-MZM structure can also display its odd-even effect. Namely, for $N \in$ odd, the zero-bias conductance values are less determined by the superconducting phases (*although θ is meaningless for $N = 1$*), whereas for $N \in$ even, the zero-bias conductances are more dependent on the superconducting phases.

Although we have presented the zero-bias conductance properties in an analytical way, the underlying physics responsible for the modification of leakage effect should be uncovered as well. According to the conclusion in Appendix B, for the case of real $\lambda_{2j-1}\lambda_{2j}^*$ and t_j, $G_{1e,1h}^r|_{\epsilon\to0} = \frac{1}{i\Gamma_L}$, and as a result, the conductance value is always manifested as $\mathbb{G}_{eV_b=0}^{LAR} = \frac{e^2}{h}$. In view of this fact, one can consider that in such a case the effective coupling between QD-2 and QD-1 is eliminated equivalently, leading to the disappearance of ET but the occurrence of resonant LAR. We would like to explain the resonant LAR as follows. In the case of $N > 1$, the multiple couplings between the MZM and the electronic and hole states provide the in-phase resonant LAR processes at the zero-energy limit. The co-occurrence of such in-phase processes in respective paths is certain to induce the constructive interference, so the LAR is enhanced to its maximum. It is not difficult to understand that once the LAR reaches its maximum, the other tunneling process, i.e., the ET, will be forbidden completely. Therefore the resonant LAR and forbidden ET should be attributed to the constructive interference among the paths contributed by the couplings between MZMs and the corresponding electronic and hole states. On the other hand, when superconducting phase differences are applied to the MZM-QD couplings, the above interference will be modified accordingly. Take the case of even N as an example. One can see that the finite superconducting phase difference is certain to take effect on the LAR and ET processes independently, so the resonant LAR will be destroyed. Otherwise, when N is odd, especially in the case of left-right ASP mode, $\lambda_{\frac{N+1}{2}}$ is real but the other MZM-QD couplings are complex; thus the tunneling path contributed by $\lambda_{\frac{N+1}{2}}$ interferes little with the other paths. As a consequence, the zero-bias conductance becomes the same as the single-QD case. A further description about this point can be found in Appendix D [46].

To better describe the zero-bias conductance results, we take the simple approach to perform the discussion by rewriting the Hamiltonian in Eq. (1) in the Majorana representation. Following the case of $N = 1$ shown in Ref. [33], we transform two metallic leads into two semi-infinite tight-binding fermionic chains, i.e., $\sum_k \varepsilon_{Lk} c_{Lk}^\dagger c_{Lk} = \sum_{j=-\infty}^{-1} \mu(c_j^\dagger c_{j-1} + \text{H.c.})$ and $\sum_k \varepsilon_{Rk} c_{Rk}^\dagger c_{Rk} = \sum_{j=N+1}^{\infty} \mu(c_j^\dagger c_{j+1} + \text{H.c.})$ ($\varepsilon_{\alpha k}$ and μ are confined by the relation of $\varepsilon_{\alpha k} = 2\mu\cos k$). Also, suppose that $d_j = c_{j-1}$, and the two leads with their connected QDs becomes a 1D chain. Next, by defining $\eta_{j1} = (c_j^\dagger + c_j)/\sqrt{2}$ and $\eta_{j2} = i(c_j^\dagger - c_j)/\sqrt{2}$, the one-dimensional chain is simplified into two Majorana chains. In the case of $\varepsilon_j = 0$, the two Majorana chains will be decoupled from each other, as shown in Fig. 4. Figure 4(a) shows that the upper chain is conducting, whereas the tunneling in the down chain is forbidden. This leads to the result of $\mathbb{G}(eV_b = 0) = \frac{e^2}{2h}$. According to this method, we can also obtain the structure schematics of $N = 2$ and 3 by considering λ_j to be real. The results are shown in Figs. 4(b) and 4(c). It is shown that MZMs are allowed to be coupled to the two chains, respectively. This certainly forbids the tunneling between the two terminals of each chain. As a result, only the local AR survives in the resonant way, and the zero-bias conductance is equal to $\frac{e^2}{h}$. Detailed descriptions can be referred in Appendix C. However, it can be anticipated
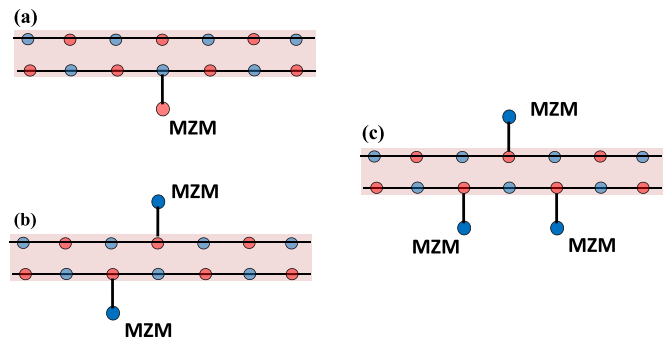

FIG. 4. Schematics of our considered structure in the Majorana representations with $N = 1, 2, 3$, in the case of real λ_j.

that in the presence of a superconducting phase difference, the above description will be modified and each MZM will be coupled to chains simultaneously, which inevitably leads to the complicated conductance results. Next in Fig. 5 we focus on the zero-bias conductance spectra of this QD-molecule structure by adjusting the superconducting phase difference in a continuous way. The structural parameters are the same as those in Figs. 2 and 3. In Fig. 5(a) where $N = 2$, we see that with the change of θ, the conductance magnitude changes in period π. When $\theta = n\pi$, the conductance magnitude reaches its maximum, whereas in the case of $\theta = (n + \frac{1}{2})\pi$, the conductance meets its minimum. What is notable is that the conductance curve is independent of the shift of QD levels. With the help of Eq. (24), we can readily understand the oscillation of the conductance curve. In Fig. 5(b) where $N = 3$, it is shown that the conductance magnitude tends to be independent of the change of superconducting phase difference, except the case of $\theta = 2n\pi$ where the resonant conductance peak comes into being. On the other hand, the results in Figs. 5(c) and 5(d) also verify our discussion about Eqs. (28) and (29). Namely, when the superconducting phase
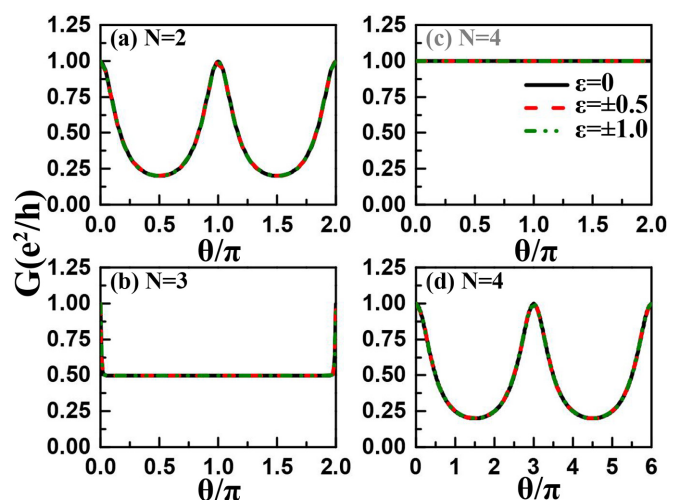

FIG. 5. Zero-bias conductance spectra of the QD-molecule structures with the change of superconducting phase difference. (a) $N = 2$ with $\lambda_1 = \lambda_2^* = \lambda_0 e^{i\theta/2}$. (b) $N = 3$ with $\lambda_1 = \lambda_3^* = \lambda_0 e^{i\theta/2}$. (c) $N = 4$ with $\lambda_{1(2)} = \lambda_{3(4)}^* = \lambda_0 e^{i\theta/2}$. (d) $N = 4$ in which $\lambda_1 = \lambda_4^* = \lambda_0 e^{i\theta/2}$ with $\lambda_2 = \lambda_3^* = \lambda_0 e^{i\theta/6}$.
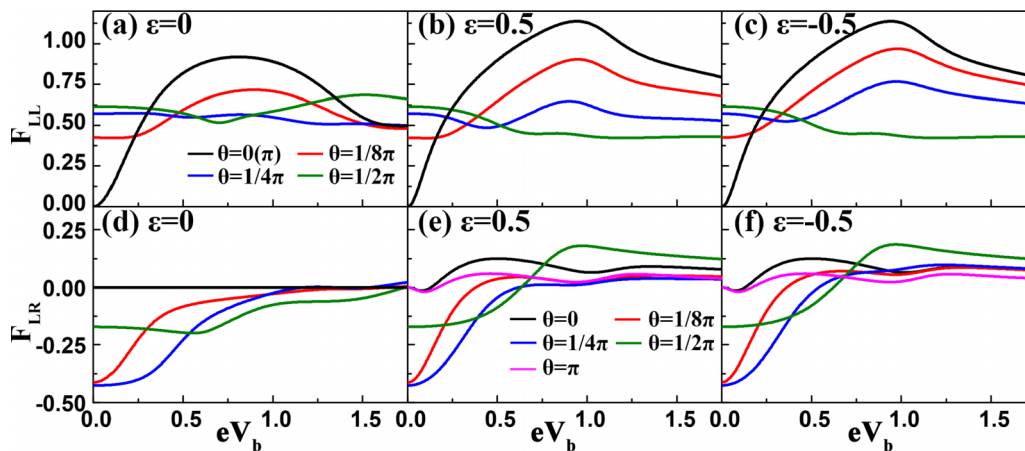
FIG. 6. Fano factors with the increase of bias voltage for the case of $N = 2$. The QD levels are taken to be $\varepsilon = 0$ and ± 0.5, respectively.

difference is partly applied with $\lambda_{1(2)} = \lambda^*_{3(4)} = \lambda_0 e^{i\theta/2}$, the conductance magnitude will be equal to $\frac{e^2}{h}$, since $\mathbb{G}^{LAR}_{V_b=0} = \frac{e^2}{h}$ and $\mathbb{G}^{ET}_{V_b=0} = 0$. As the superconducting phase difference is applied fully, the maximum value of the zero-bias conductance is $\frac{e^2}{h}$ and the minimum value is $\frac{0.2e^2}{h}$, which is the same as the result of $N = 2$. However, the zero-bias conductance displays the period 3π in Fig. 5(d).

In order to further understand the conductance properties, the Fano factors are worth exploring in detail which describe the tunneling characteristics of quasiparticles. Therefore we focus on the change of Fano factors following the increase of QD number or superconducting phase difference. For the structure of $N = 2$, the results of F_{LL} are shown in Figs. 6(a)–6(c), and those of F_{LR} are shown in Figs. 6(d)–6(f), respectively. In Fig. 6(a) we see that when QD levels are fixed at zero, the value of F_{LL} increases obviously from zero with $\theta = 0$ and $\theta = \pi$, whereas the value of $F_{LL}(V_b = 0)$ increases with the presence of the superconducting phase difference. Thereafter, it oscillates following the increase of the bias voltage. At the large-bias limit, F_{LL} almost keeps close to 0.5, except for the case of $\theta = \frac{\pi}{2}$. Next, in Figs. 6(b) and 6(c), it shows that when QD levels deviate from zero, the Fano factor at the zero-bias limit does not change, identical with the result of $\varepsilon = 0$. In the finite-bias region, the magnitude of F_{LL} begins to depend on the sign of ε, but the variation manners in these two cases are basically similar to each other. In Figs. 6(d)–6(f) we present the spectra of F_{LR}, the parameters of which are the same as Figs. 6(a)–6(c), respectively. Figure 6(d) shows that at $\varepsilon = 0$, F_{LR} is always at 0, and there is no fluctuation with $\theta = 0$ and $\theta = \pi$. Then its value at zero-bias limit with $\frac{\pi}{8}$ is equal to the value at $\theta = \frac{\pi}{4}$. It can also observed that regardless of the superconducting phase difference, the value of F_{LR} is near 0 at the large-bias limit. In Figs. 6(e) and 6(f) it can be found that in the cases of $\varepsilon = \pm 0.5$, the values of F_{LR} are equal at zero-bias limit when the superconducting phase difference is taken to be 0 and π ($\frac{\pi}{8}$ and $\frac{\pi}{4}$), respectively. After that, their variation tendencies become dependent on the superconducting phase difference. We therefore understand that in the case of $N = 2$ with the finite superconducting phase difference, the zero-bias Fano factors seem to be irrelevant to the conductance, and also,

F_{LL} and F_{LR} are not related to each other at the zero-bias limit.

The results of Fano factors with $N = 3$ are shown in Fig. 7. For F_{LL}, when $\theta = 0$, its value is improved from zero with the increase of bias voltage. In the presence of a superconducting phase difference, the value of F_{LL} starts to vary from 0.5. We thus ascertain that at the zero-bias limit, $F_{LL}(V_b = 0) = 1 - \mathcal{T}|_{\varepsilon=V_b=0}$. It is shown in Fig. 7(a) at $\theta = \frac{\pi}{4}$ that after a series of oscillations it will return to about 0.5 when $eV_b = 2.0$, which is equal to $eV_b = 0$. When $eV_b > 1.0$, the change trend of $\theta = 0$ and $\theta = \frac{\pi}{8}$ is consistent. In addition, it is not difficult to observe that the maximum value of F_{LL} exceeds 1.25 at $eV_b = 1.0$ when the superconducting phase difference is zero. Meanwhile, the value of F_{LL} decreases in the range of $1.0 < eV_b < 2.0$. In Fig. 7(c) the change of F_{LL} at $\varepsilon = -0.5$ is not much different from that at $\varepsilon = 0.5$. Next we present the corresponding F_{LR} in Figs. 7(d)–7(f). It can be found that when $\theta = 0$, no matter what value of the QD level takes, F_{LR} has little change and is always close to 0. This shows that the QD level has no effect on F_{LR}. In the following when $\theta = \frac{\pi}{8}$, the value of $F_{LR}(V_b = 0)$ can almost reach about 0.5, but the further increase of θ tends to suppress this value. Therefore in the case of $N = 3$, one can only find the clear relationship between the conductance and F_{LL} at the zero-bias limit.

To see the change of Fano factors at the zero-bias limit more intuitively, we present the variation of the Fano factors regarding the superconducting phase difference, as shown in Fig. 8. In the case of $N = 2$ it can be observed that F_{LL} changes in period π with the increase of superconducting phase difference. Thus the relationship of F_{LL} satisfies $F_{LL}(\theta) = F_{LL}(\pi - \theta)$. When $\theta = n\pi$, F_{LL} becomes equal to zero. The notable phenomenon is that the change of F_{LL} is opposite to the conductance in Fig. 4(a). However, the relationship of $F_{LL}(V_b = 0) = 1 - \mathcal{T}|_{\varepsilon=V_b=0}$ only appears at the case of $\theta = n\pi$. For F_{LR} in Fig. 8(b), its spectrum oscillates seriously with the increase of superconducting phase difference, though it satisfies $F_{LR}(\theta) = F_{LR}(\pi - \theta)$. This also shows that in the case of $\theta \neq n\pi$, the relationship between F_{LL} and F_{LR} cannot be described quantitatively. The reason should be attributed to the varied contributions of the ET and local AR for respective θ. On the other hand, for $N = 3$ in Fig. 8(c) we see that except for $\theta = 0$ and $\theta = 2\pi$, F_{LL} is fixed at 0.5.
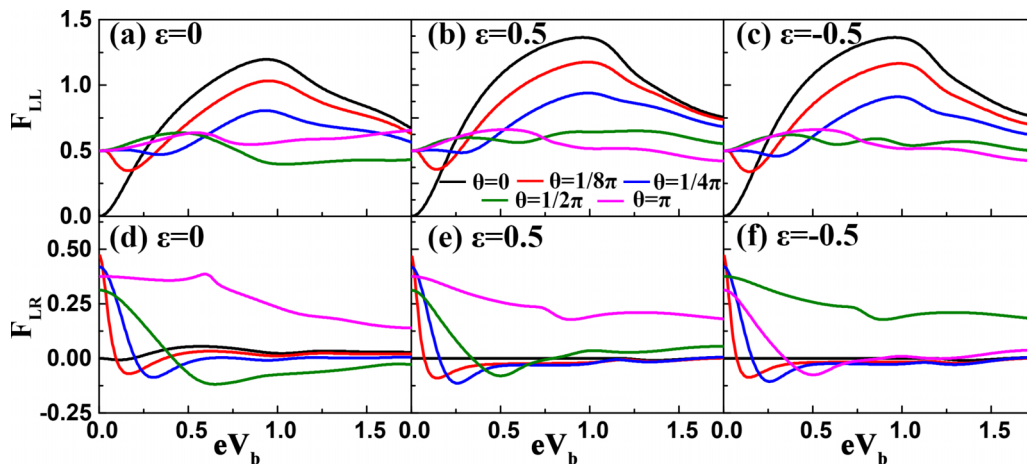
FIG. 7. Fano factors with the increase of bias voltage for the case of $N = 3$. The QD levels are taken to be $\varepsilon = 0$ and ± 0.5, respectively.

After comparing with the conductance result, one can get the relation of $F_{LL}(V_b = 0) = 1 - \mathcal{T}|_{\epsilon = V_b = 0}$. This result seems to describe a single-particle tunneling result. As a matter of fact, this originates from the equal contribution of the ET and local AR, accordant with the result of single QD. Next, in Fig. 8(d) it shows that the curve of F_{LR} displays weak oscillation following the increase of the superconducting phase difference in its period 2π. This exhibits an alternative relationship between F_{LL} and F_{LR}. Up to now we know that the zero-bias Fano factors also display their odd-even effects, namely, the oscillation manners of $F_{L\alpha}(V_b = 0)$ depend on the parity of the QD number. Meanwhile, the odd-N cases possess the well-defined relationship between the zero-bias conductance and F_{LL}.

IV. SUMMARY

To summarize, we have performed the investigation about the electron transport through a QD molecule in which the
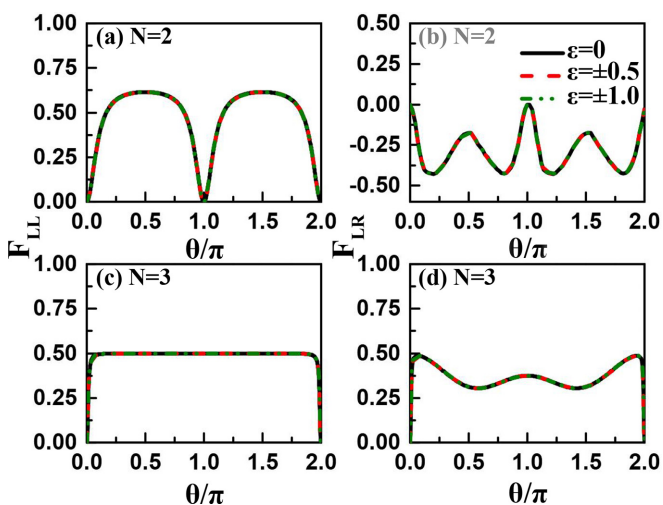

FIG. 8. Zero-bias Fano factors with the change of superconducting phase difference. (a), (b) Results of F_{LL} and F_{LR} for $N = 2$. (c), (d) Results of $N = 3$.

serially coupled QDs are side-coupled to MZMs at the ends of TS nanowires. After calculation we found that in this structure with $N > 1$, following the increase of QD number, the zero-bias conductance does not display the conventional odd-even effect but always keeps equal to $\frac{e^2}{h}$. On the other hand, when finite superconducting phase differences among MZMs are taken into account, the zero-bias conductance can be modulated in an efficient way which is also determined by the parity of the QD number and the appearance manner of superconducting phases. Specifically, if different superconducting phases are added to the QD-MZM couplings according to the left-right ASP mode, the zero-bias conductances will display apparent odd-even effect. Namely, in the odd-QD cases, the zero-bias conductances are less determined by the superconducting phase, whereas they are more dependent on the superconducting phase in the cases of even QDs. In addition to the conductances, the shot-noise Fano factors also display odd-even effects, since their dependences on the superconducting phase difference are determined by the parity of QD number. To be specific, the QD-number parity is able to affect the interplay between the ET and local AR processes in a substantial way. We anticipate that these results are helpful to construct mesoscopic cells based on QDs and MZMs.

APPENDIX A: GREEN FUNCTIONS FOR LAR

As shown in Fig. 1(b), our considered structure can be transformed into a four-terminal serially coupled configuration in each cell of which three "atoms" are coupled serially.

Then we are allowed to deduce the analytical expression of the Green functions related to the LAR. To begin with, the Hamiltonian of the jth cell is written as

$$h_j = \begin{bmatrix} \varepsilon_j & \lambda_j^* & 0 \\ \lambda_j & 0 & -\lambda_j^* \\ 0 & -\lambda_j & -\varepsilon_j \end{bmatrix}. \tag{A1}$$

According to the Dyson equation, the Green function in the jth cell can be directly expressed, i.e.,

$$G_j^r = [\epsilon + i0^+ - h_j - \Sigma_j]^{-1}, \tag{A2}$$

where $\Sigma_j = \mathcal{H}_{tj}^* G_{j+1}^r \mathcal{H}_{tj}$ for $j < N$. Σ_j is so-called self-energy term, and $\mathcal{H}_{tj}$ is the matrix of the coupling Hamiltonian between two neighboring cells. According to Fig. 1(b) and Eq. (10), we know that

$$\mathcal{H}_{tj} = \begin{bmatrix} t_j & 0 & 0 \\ 0 & 0 & 0 \\ 0 & 0 & -t_j^* \end{bmatrix}. \tag{A3}$$

Thus the expression form of self-energy is

$$\Sigma_j = \begin{bmatrix} \Sigma_{j,11} & 0 & \Sigma_{j,13} \\ 0 & 0 & 0 \\ \Sigma_{j,31} & 0 & \Sigma_{j,33} \end{bmatrix}, \tag{A4}$$

in which

$$\Sigma_{j,11} = \frac{|t_j|^2}{\mathcal{D}_{j+1}}[\epsilon(\epsilon + \varepsilon_{j+1} - \Sigma_{j+1,33}) - |\lambda_{j+1}|^2],$$

$$\Sigma_{j,13} = \frac{(t_j^*)^2}{\mathcal{D}_{j+1}}[(\lambda_{j+1}^*)^2 - \epsilon\Sigma_{j+1,13}],$$

$$\Sigma_{j,31} = \frac{(t_j)^2}{\mathcal{D}_{j+1}}[(\lambda_{j+1})^2 - \epsilon\Sigma_{j+1,31}],$$

$$\Sigma_{j,33} = \frac{t_j^2}{\mathcal{D}_{j+1}}[\epsilon(\epsilon - \varepsilon_{j+1} - \Sigma_{j+1,11}) - |\lambda_{j+1}|^2], \tag{A5}$$

with $\mathcal{D}_j = \det |[G_j^r]^{-1}|$. Note, also, that the Nth cell is coupled to lead R, and the nonzero elements of Σ_N are given as $\Sigma_{N,11} = \Sigma_{N,33} = -\frac{i}{2}\Gamma_R$. Following the above deduction, the Green function matrix of the first cell can be expressed as

$$\begin{aligned} &[G_1^r]^{-1} \\ &= \begin{bmatrix} \epsilon - \varepsilon_1 + \frac{i}{2}\Gamma_L - \Sigma_{1,11} & -\lambda_1^* & \Sigma_{1,13} \\ -\lambda_1 & \epsilon & \lambda_1^* \\ \Sigma_{1,31} & \lambda_1 & \epsilon + \varepsilon_1 + \frac{i}{2}\Gamma_L - \Sigma_{1,33} \end{bmatrix}. \end{aligned} \tag{A6}$$

As a typical case, in the limit of $\epsilon \to 0$ we have

$$G_{1e,1h}^r|_{\epsilon\to0} = \frac{-(\lambda_1^*)^2}{-i\Gamma_L|\lambda_1|^2 + [(\lambda_1^*)^2\Sigma_{1,31} + \lambda_1^2\Sigma_{1,13} + |\lambda_1|^2(\Sigma_{1,11} + \Sigma_{1,33})]}. \tag{A7}$$

Take the case of $N = 2$ as an example, where the Green function contributing to the LAR process is given as

$$G_{1e,1h}^r|_{\epsilon\to0} = \frac{i\Gamma_R\lambda_1^2|\lambda_2|^2}{-\Gamma_L\Gamma_R|\lambda_1|^2|\lambda_2|^2 + |t_1|^2(\lambda_1^*\lambda_2 - \lambda_1\lambda_2^*)^2}. \tag{A8}$$

When $N = 3$, the Green functions contributing to the LAR process can be expressed as

$$G_{1e,1h}^r|_{\epsilon\to0} = \frac{\lambda_1^2|t_2|^2(\lambda_2^*\lambda_3 - \lambda_2\lambda_3^*)^2}{\Lambda_3}, \tag{A9}$$

with $\Lambda_3 = \det |[\mathbf{G}^r|_{\epsilon=0}]^{-1}| = i\Gamma_L|\lambda_1|^2|t_2|^2(\lambda_2^*\lambda_3 - \lambda_2\lambda_3^*)^2 + i\Gamma_R|t_1|^2(\lambda_1^*\lambda_2 - \lambda_1\lambda_2^*)^2|\lambda_3|^2$. Next, in the case of $N = 4$, the corresponding Green function at the limit of $\epsilon \to 0$ can be written as

$$G_{1e,1h}^r|_{\epsilon\to0} = \frac{i\Gamma_R\lambda_1^2|t_2|^2(\lambda_2^*\lambda_3 - \lambda_2\lambda_3^*)^2|\lambda_4|^2}{\Lambda_4}, \tag{A10}$$

with $\Lambda_4 = -\Gamma_L\Gamma_R|\lambda_1|^2|t_2|^2(\lambda_2^*\lambda_3 - \lambda_2\lambda_3^*)^2|\lambda_4|^2 + |t_1|^2(\lambda_1^*\lambda_2 - \lambda_1\lambda_2^*)^2|t_3|^2(\lambda_3^*\lambda_4 - \lambda_3\lambda_4^*)^2$. When trying to summarize the general forms of $G_{1e,1h}^r|_{\epsilon\to0}$, we find that if $N = odd$ $(N > 1)$,

$$G_{1e,1h}^r|_{\epsilon\to0} = \frac{1}{\Lambda_N}\lambda_1^2|t_2|^2(\lambda_2^*\lambda_3 - \lambda_2\lambda_3^*)^2 \cdots$$
$$\times |t_{N-1}|^2(\lambda_{N-1}^*\lambda_N - \lambda_{N-1}\lambda_N^*)^2, \tag{A11}$$

with $\Lambda_N = i\Gamma_L|\lambda_1 t_2|^2(\lambda_2^*\lambda_3 - \lambda_2\lambda_3^*)^2 \cdots |t_{N-1}|^2(\lambda_{N-1}^*\lambda_N - \lambda_{N-1}\lambda_N^*)^2 + i\Gamma_R|t_1|^2(\lambda_1^*\lambda_2 - \lambda_1\lambda_2^*)^2 \cdots |t_{N-2}|^2(\lambda_{N-2}^*\lambda_{N-1} - \lambda_{N-2}\lambda_{N-1}^*)^2|\lambda_N|^2$. If $N = even$,

$$G_{1e,1h}^r|_{\epsilon\to0} = \frac{i\Gamma_R}{\Lambda_N}\lambda_1^2|t_2|^2(\lambda_2^*\lambda_3 - \lambda_2\lambda_3^*)^2 \cdots$$
$$\times (\lambda_{N-1}^*\lambda_N - \lambda_{N-1}\lambda_N^*)^2|\lambda_N|^2, \tag{A12}$$

with $\Lambda_N = -\Gamma_L\Gamma_R|\lambda_1 t_2|^2(\lambda_2^*\lambda_3 - \lambda_2\lambda_3^*)^2 \cdots |t_{N-2}|^2(\lambda_{N-2}\lambda_{N-1} - \lambda_{N-2}\lambda_{N-1}^*)^2|\lambda_N|^2 + |t_1|^2(\lambda_1^*\lambda_2 - \lambda_1\lambda_2^*)^2 \cdots |t_{N-1}|^2(\lambda_{N-1}^*\lambda_N - \lambda_{N-1}\lambda_N^*)^2$.

On the other hand, for the case of real $\lambda_{2j-1}\lambda_{2j}^*$ and t_j, the Green function matrix in Eq. (A7) can be further simplified, i.e.,

$$\begin{aligned} G_{1e,1h}^r|_{\epsilon\to0} &= \frac{1}{i\Gamma_L - [\Sigma_{1,31} + \Sigma_{1,13} + \Sigma_{1,11} + \Sigma_{1,33}]} \\ &= \frac{1}{i\Gamma_L}, \end{aligned} \tag{A13}$$

because of $\Sigma_{1,mm'} = -\Sigma_{1,mm}$. This exactly leads to the result of $\mathbb{G}_{V_b=0}^{AR} = \frac{e^2}{h}$.

APPENDIX B: GREEN FUNCTIONS OF ET

For describing the ET between the two metallic leads, we would like to divide the structure in Fig. 1(b) into three

parts, i.e., the electron, MZM, and hole parts. Accordingly, the system Hamiltonian should be written as

$$
H = \begin{bmatrix} H_e & H_{eM} & 0 \\ H_{eM}^\dagger & H_M & H_{Mh} \\ 0 & H_{Mh}^\dagger & H_h \end{bmatrix}.
\tag{B1}
$$

H_e, H_M, and H_h correspond to the Hamiltonians of these three parts, respectively. They are

$$
H_e = \begin{bmatrix}
\varepsilon_1 & t_1 & 0 & \cdots & 0 \\
t_1^* & \varepsilon_2 & t_2 & 0 & \vdots \\
0 & \cdots & \ddots & \cdots & 0 \\
\vdots & \cdots & t_{N-2}^* & \varepsilon_{N-1} & t_{N-1} \\
0 & \cdots & 0 & t_{N-1}^* & \varepsilon_N
\end{bmatrix}
\tag{B2}
$$

and

$$
H_h = \begin{bmatrix}
-\varepsilon_1 & -t_1^* & 0 & \cdots & 0 \\
t_1 & -\varepsilon_2 & t_2 & 0 & \vdots \\
0 & \cdots & \ddots & \cdots & 0 \\
\vdots & \cdots & -t_{N-2} & -\varepsilon_{N-1} & -t_{N-1}^* \\
0 & \cdots & 0 & -t_{N-1} & -\varepsilon_N
\end{bmatrix}
\tag{B3}
$$

with $H_{M,jl} = 0$. Meanwhile, H_{eM} and H_{Mh} denote the coupling matrices between the two neighboring parts, which are given as

$$
H_{eM} = \begin{bmatrix}
\lambda_1^* & 0 & 0 & \cdots & 0 \\
0 & \lambda_2^* & 0 & 0 & \vdots \\
0 & \cdots & \ddots & \cdots & 0 \\
\vdots & \cdots & 0 & \lambda_{N-1}^* & 0 \\
0 & \cdots & 0 & 0 & \lambda_N^*
\end{bmatrix}
\tag{B4}
$$

and

$$
H_{Mh} = \begin{bmatrix}
-\lambda_1^* & 0 & 0 & \cdots & 0 \\
0 & -\lambda_2^* & 0 & 0 & \vdots \\
0 & \cdots & \ddots & \cdots & 0 \\
\vdots & \cdots & 0 & -\lambda_{N-1}^* & 0 \\
0 & \cdots & 0 & 0 & -\lambda_N^*
\end{bmatrix}.
\tag{B5}
$$

With the help of the above matrix results, the Green function of the electron part can be defined as

$$
G_e^r = \left[\epsilon + i0^+ - H_e - H_{eM}^\dagger G_M^r H_{eM} - \Sigma_e\right]^{-1},
\tag{B6}
$$

in which

$$
\begin{aligned}
G_M^r &= \left[\epsilon + i0^+ - H_M - H_{Mh}G_h^r H_{Mh}^\dagger\right]^{-1}, \\
G_h^r &= \left[\epsilon + i0^+ - H_h - \Sigma_h\right]^{-1}.
\end{aligned}
\tag{B7}
$$

In our system it can be considered that $\Sigma_{e,jl} = \Sigma_{h,jl} = \frac{i}{2}\Gamma_L\delta_{j1}\delta_{l1} + \frac{i}{2}\Gamma_R\delta_{jN}\delta_{lN}$, since the metallic leads are supposed to be fabricated by the two-dimensional electron gas.

Following the above theory, the Green functions related to the ET between the two leads can be solved analytically. First, in the case of $N = 2$ one can readily obtain the result that

$$
G_{1e,2e}^r|_{\epsilon\to0} = \frac{t_1^*\lambda_1\lambda_2^*(\lambda_1^*\lambda_2 - \lambda_1\lambda_2^*)}{-\Gamma_L\Gamma_R|\lambda_1|^2|\lambda_2|^2 + |t_1|^2(\lambda_1^*\lambda_2 - \lambda_1\lambda_2^*)^2}.
\tag{B8}
$$

Regarding the case of $N = 3$, the Green functions contributing to the ET process can be expressed as

$$
G_{1e,3e}^r|_{\epsilon\to0} = \frac{\lambda_1\lambda_3^*t_1^*t_2^*(\lambda_1^*\lambda_2 - \lambda_1\lambda_2^*)(\lambda_2^*\lambda_3 - \lambda_2\lambda_3^*)}{\Lambda_3}.
\tag{B9}
$$

Next, when this system is increased to $N = 4$, the Green function at the limit of $\epsilon \to 0$ can be written as

$$
\begin{aligned}
G_{1e,4e}^r|_{\epsilon\to0} &= \frac{\lambda_1\lambda_4^*t_1^*t_2^*t_3^*}{\Lambda_4}(\lambda_1^*\lambda_2 - \lambda_1\lambda_2^*) \\
&\times (\lambda_2^*\lambda_3 - \lambda_2\lambda_3^*)(\lambda_3^*\lambda_4 - \lambda_3\lambda_4^*).
\end{aligned}
\tag{B10}
$$

In view of the results in Eqs. (B8)–(B10), we can summarize the generalized expressions of $G_{1e,Ne}^r|_{\epsilon\to0}$, i.e.,

$$
\begin{aligned}
G_{1e,Ne}^r|_{\epsilon\to0} &= \frac{\lambda_1\lambda_N^*t_1^*\cdots t_{N-1}^*}{\Lambda_N}(\lambda_1^*\lambda_2 - \lambda_1\lambda_2^*) \\
&\times (\lambda_2^*\lambda_3 - \lambda_2\lambda_3^*)\cdots(\lambda_{N-1}^*\lambda_N - \lambda_{N-1}\lambda_N^*).
\end{aligned}
\tag{B11}
$$

Note that the forms of Λ_N are accordant with those in Eqs. (A11) and (A12), respectively, determined by the parity of N. It shows that at the limit of $\epsilon \to 0$, the above retarded Green functions become irrelevant to the QD levels but are determined by the inter-QD and QD-MZM couplings. It should be noted that in the case of real $\lambda_{2j-1}\lambda_{2j}^*$, there will be $G_{1e,Ne}^r|_{\epsilon\to0} = 0$. And then, at the zero-bias limit, the ET conductance will be manifested as $\mathbb{G}_{V_b=0}^{ET} = 0$.

APPENDIX C: RELATIONSHIPS OF GREEN FUNCTIONS IN NAMBU AND MAJORANA REPRESENTATIONS

For our structure, when we define $d_j = c_{j-1}$ with $\eta_{j1} = (c_j^\dagger + c_j)/\sqrt{2}$ and $\eta_{j2} = i(c_j^\dagger - c_j)/\sqrt{2}$, it can be transformed into Majorana chains shown in Fig. 4. And then the relationships of Green functions in Nambu and Majorana representations can be presented for further understanding the conductance results. For instance, in the case of $N = 1$, we can find that

$$
\begin{aligned}
G_{1e,1e}^r &= \langle\!\langle d_1|d_1^\dagger\rangle\!\rangle \\
&= \frac{1}{2}\langle\!\langle \eta_{01}|\eta_{01}\rangle\!\rangle - \frac{i}{2}\langle\!\langle \eta_{01}|\eta_{02}\rangle\!\rangle \\
&\quad + \frac{i}{2}\langle\!\langle \eta_{02}|\eta_{01}\rangle\!\rangle + \frac{1}{2}\langle\!\langle \eta_{02}|\eta_{02}\rangle\!\rangle,
\end{aligned}
\tag{C1}
$$

$$
\begin{aligned}
G_{1e,1h}^r &= \langle\!\langle d_1|d_1\rangle\!\rangle \\
&= \frac{1}{2}\langle\!\langle \eta_{01}|\eta_{01}\rangle\!\rangle + \frac{i}{2}\langle\!\langle \eta_{01}|\eta_{02}\rangle\!\rangle \\
&\quad + \frac{i}{2}\langle\!\langle \eta_{02}|\eta_{01}\rangle\!\rangle - \frac{1}{2}\langle\!\langle \eta_{02}|\eta_{02}\rangle\!\rangle.
\end{aligned}
\tag{C2}
$$

As a typical case where $\varepsilon = 0$, the two Majorana chains are decoupled from each other at the zero-energy limit, thus

$$\langle\langle d_1|d_1^\dagger\rangle\rangle = \frac{1}{2}\langle\langle\eta_{01}|\eta_{01}\rangle\rangle + \frac{1}{2}\langle\langle\eta_{02}|\eta_{02}\rangle\rangle,$$

$$\langle\langle d_1^\dagger|d_1^\dagger\rangle\rangle = \frac{1}{2}\langle\langle\eta_{01}|\eta_{01}\rangle\rangle - \frac{1}{2}\langle\langle\eta_{02}|\eta_{02}\rangle\rangle. \tag{C3}$$

Due to the presence of one side-coupled Majorana site in the down branch [see Fig. 4(a) in the manuscript], $\langle\langle\eta_{02}|\eta_{02}\rangle\rangle|_{\varepsilon=0}$ will be equal to zero. As a result,

$$\langle\langle d_1|d_1^\dagger\rangle\rangle|_{\varepsilon=0} = \langle\langle d_1|d_1\rangle\rangle|_{\varepsilon=0}$$
$$= \frac{1}{2}\langle\langle\eta_{01}|\eta_{01}\rangle\rangle|_{\varepsilon=0}. \tag{C4}$$

Following this analysis, one can find that the ET and LAR correspond to the particle tunneling in the upper branch. From the above equations we can understand the halved conductance value at the zero-bias limit.

Based on the above idea, we can analyze the case of $N = 2$. To be specific, the Green functions involved can be expressed as

$$G_{1e,2e}^r = \langle\langle d_1|d_2^\dagger\rangle\rangle$$
$$= \frac{1}{2}\langle\langle\eta_{01}|\eta_{11}\rangle\rangle - \frac{i}{2}\langle\langle\eta_{01}|\eta_{12}\rangle\rangle$$
$$+ \frac{i}{2}\langle\langle\eta_{02}|\eta_{11}\rangle\rangle + \frac{1}{2}\langle\langle\eta_{02}|\eta_{12}\rangle\rangle, \tag{C5}$$

$$G_{1e,1h}^r = \langle\langle d_1|d_1\rangle\rangle$$
$$= \frac{1}{2}\langle\langle\eta_{01}|\eta_{01}\rangle\rangle + \frac{i}{2}\langle\langle\eta_{01}|\eta_{02}\rangle\rangle$$
$$+ \frac{i}{2}\langle\langle\eta_{02}|\eta_{01}\rangle\rangle - \frac{1}{2}\langle\langle\eta_{02}|\eta_{02}\rangle\rangle. \tag{C6}$$

At the case of $\varepsilon = 0$,

$$\langle\langle d_1|d_2^\dagger\rangle\rangle = \frac{1}{2}\langle\langle\eta_{01}|\eta_{11}\rangle\rangle + \frac{1}{2}\langle\langle\eta_{02}|\eta_{12}\rangle\rangle,$$

$$\langle\langle d_1^\dagger|d_1^\dagger\rangle\rangle = \frac{1}{2}\langle\langle\eta_{01}|\eta_{01}\rangle\rangle - \frac{1}{2}\langle\langle\eta_{02}|\eta_{02}\rangle\rangle. \tag{C7}$$

With the geometry of the Majorana chains in Fig. 4(b) of the manuscript, we know

$$\langle\langle d_1|d_2^\dagger\rangle\rangle|_{\varepsilon=0} = 0,$$

$$\langle\langle d_1|d_1\rangle\rangle|_{\varepsilon=0} = \frac{1}{2}\langle\langle\eta_{01}|\eta_{01}\rangle\rangle|_{\varepsilon=0}. \tag{C8}$$

Note that due to $\langle\langle\eta_{01}|\eta_{11}\rangle\rangle|_{\varepsilon=0} = 0$, $\langle\langle\eta_{01}|\eta_{01}\rangle\rangle|_{\varepsilon=0}$ is actually the surface Green function of the semi-infinite Majorana chain at the zero-energy limit, and it can describe the resonant AR. Therefore, in the case of $N = 2$, only the LAR survives in the resonant way, and the zero-bias conductance is equal to e^2/h. These analysis can be helpful in understanding the complicate structures with larger N.

APPENDIX D: DESCRIPTION ABOUT CONDUCTANCES MODULATED BY THE PHASES OF MZM-QD COUPLINGS

Regarding the phases of the coupling coefficients between the QDs and the corresponding MZMs, we consider that the MZMs can be generated at the ends of a multiterminal nanowire. When they are coupled to the QDs, one multiring structure is constructed, and then the phases of the QD-MZM couplings can be realized by introducing finite local magnetic fluxes through this structure.

For the triple-QD structure, when local magnetic fluxes Φ_1 and Φ_2 thread through its two subrings, the QD-MZM couplings will get their phase factors as $\lambda_1 = |\lambda_1|e^{i(\phi_1+\phi_2)}$, $\lambda_2 = |\lambda_2|e^{i(-\phi_1+\phi_2)}$, and $\lambda_3 = |\lambda_3|e^{-i(\phi_1+\phi_2)}$, where $\phi_j = 2\pi\Phi_j/\phi_0$, with $\phi_0 = h/e$ being the magnetic flux quantum. Therefore, under such an assumption, the expressions for the conductance components at the zero-bias limit are

$$\mathbb{G}_{eV_b=0}^{\text{LAR}} = \frac{e^2}{h}\frac{\Gamma_L^2|t_2|^4\sin^4 2\phi_1}{|\Gamma_L|t_2|^2\sin^2 2\phi_1 + \Gamma_R|t_1|^2\sin^2 2\phi_2|^2},$$

$$\mathbb{G}_{eV_b=0}^{ET} = \frac{e^2}{h}\frac{\Gamma_L\Gamma_R\sin^2 2\phi_1\sin^2 2\phi_2}{|\Gamma_L|t_2|^2\sin^2 2\phi_1 + \Gamma_R|t_1|^2\sin^2 2\phi_2|^2},$$
$$[\mathbf{N = 3}]. \tag{D1}$$

From the above equation one sees that the two conductances are dependent on the phase factors. As a typical case where $t_1 = t_2$ and $\Gamma_L = \Gamma_R$, they read

$$\mathbb{G}_{eV_b=0}^{\text{LAR}} = \frac{e^2}{h}\frac{\sin^4 2\phi_1}{(\sin^2 2\phi_1 + \sin^2 2\phi_2)^2},$$

$$\mathbb{G}_{eV_b=0}^{ET} = \frac{e^2}{h}\frac{\sin^2 2\phi_1\sin^2 2\phi_2}{(\sin^2 2\phi_1 + \sin^2 2\phi_2)^2}, \quad [\mathbf{N = 3}]. \tag{D2}$$

On the other hand, in the case of $\phi_1 = \phi_2$, the zero-bias conductances of Eq. (D1) can be expressed as

$$\mathbb{G}_{eV_b=0}^{\text{LAR}} = \frac{e^2}{h}\frac{\Gamma_L^2|\lambda_1 t_2|^4}{|\Gamma_L|\lambda_1 t_2|^2 + \Gamma_R|\lambda_3 t_1|^2|^2},$$

$$\mathbb{G}_{eV_b=0}^{ET} = \frac{e^2}{h}\frac{\Gamma_L\Gamma_R|\lambda_1\lambda_3 t_1 t_2|^2}{|\Gamma_L|\lambda_1 t_2|^2 + \Gamma_R|\lambda_3 t_1|^2|^2}, \quad [\mathbf{N = 3}]. \tag{D3}$$

Under the condition of $t_1 = t_2$, $|\lambda_1| = |\lambda_3|$, and $\Gamma_L = \Gamma_R$, there will be $\mathbb{G}_{eV_b=0}^{\text{LAR}} = \frac{e^2}{4h}$ and $\mathbb{G}_{eV_b=0}^{ET} = \frac{e^2}{4h}$.

For the four-QD structure, we are allowed to take local magnetic fluxes Φ_1, Φ_2, and Φ_3 and thread through its three subrings. Therefore, the QD-MZM couplings are $\lambda_1 = |\lambda_1|e^{i(\phi_1+\phi_2+\phi_3)}$, $\lambda_2 = |\lambda_2|e^{i(-\phi_1+\phi_2+\phi_3)}$, $\lambda_3 = |\lambda_2|e^{i(-\phi_1-\phi_2+\phi_3)}$, and $\lambda_4 = |\lambda_4|e^{-i(\phi_1+\phi_2+\phi_3)}$. Under this condition, the zero-bias conductance expressions can be written as

$$\mathbb{G}_{eV_b=0}^{ET} = \frac{e^2}{h}\frac{4\Gamma_L\Gamma_R|t_1 t_2 t_3|^2\sin^2 2\phi_1\sin^2 2\phi_2\sin^2 2\phi_3}{\Omega_1},$$

$$\mathbb{G}_{eV_b=0}^{\text{LAR}} = \frac{e^2}{h}\frac{\Gamma_L^2\Gamma_R^2|t_2|^4\sin^4 2\phi_2}{\Omega_1}, \quad [\mathbf{N = 4}]. \tag{D4}$$

In the above equations, $\Omega_1 = |\Gamma_L\Gamma_R|t_2|^2\sin^2 2\phi_2 + 4|t_1 t_3|^2\sin^2 2\phi_1\sin^2 2\phi_3|^2$. It can be found that in comparison with ϕ_1 and ϕ_3, ϕ_2 plays its dominant role in governing the conductance components, especially the LAR conductance. Following this fact, we would like to pay attention to the case of $\phi_1 = \phi_3$. In this case the QD-MZM couplings are $\lambda_1 = |\lambda_1|e^{i(2\phi_1+\phi_2)}$, $\lambda_2 = |\lambda_2|e^{i\phi_2}$, $\lambda_3 = |\lambda_2|e^{-i\phi_2}$, and $\lambda_4 = |\lambda_4|e^{-i(2\phi_1+\phi_2)}$. So, conductance at the zero-bias limit can be rewritten as

$$\mathbb{G}_{eV_b=0}^{ET} = \frac{e^2}{h}\frac{4\Gamma_L\Gamma_R|t_1 t_2 t_3|^2\sin^4 2\phi_1\sin^2 2\phi_2}{\Omega_2},$$

$$\mathbb{G}_{eV_b=0}^{\text{LAR}} = \frac{e^2}{h}\frac{\Gamma_L^2\Gamma_R^2|t_2|^4\sin^4 2\phi_2}{\Omega_2}, \quad [\mathbf{N = 4}]. \tag{D5}$$

$\Omega_2 = |\Gamma_L \Gamma_R |t_2|^2 \sin^2 2\phi_2 + 4|t_1 t_3|^2 \sin^4 2\phi_1|^2$. It is not difficult to find that the conductances are effected by the phase factors. When the parameters satisfy $t_j = t$ and $\Gamma_L = \Gamma_R = \Gamma$, the conductances at the zero-bias limit can be simplified as

$$\mathbb{G}^{ET}_{eV_b=0} = \frac{e^2}{h} \frac{4\Gamma^4 \sin^4 2\phi_1 \sin^2 2\phi_2}{(\Gamma^2 \sin^2 2\phi_2 + 4t^2 \sin^4 2\phi_1)^2},$$

$$\mathbb{G}^{LAR}_{eV_b=0} = \frac{e^2}{h} \frac{\Gamma^4 \sin^4 2\phi_2}{(\Gamma^2 \sin^2 2\phi_2 + 4t^2 \sin^4 2\phi_1)^2}, \quad [\mathbf{N=4}].$$

$$(D6)$$

Analogous to the case of $N = 3$, in this case we have taken two configurations. For the first case of $\lambda_1 = \lambda_4 = \lambda_0 e^{i\theta/2}$ and $\lambda_2 = \lambda_3^* = \lambda_0 e^{i\theta/6}$, it can be experimentally achieved by taking $\phi_1 = \phi_2 = \phi_3 = \frac{\theta}{6}$. For the other case where $\lambda_{1(2)} = \lambda_0 e^{i\theta/2} = \lambda_{3(4)}^*$, the magnetic fluxes should obey the relationship of $\phi_1 = \phi_3 = 0$ and $\phi_2 = \frac{\theta}{2}$. Under this condition there will be $\mathbb{G}^{LAR}_{V_b=0} = \frac{e^2}{h}$ and $\mathbb{G}^{ET}_{V_b=0} = 0$. It can found that regardless of the different phase factors, the odd-even effect of the conductance is always notable. One can further understand the changes of the conductance magnitudes following the variation of relevant parameters.

[1] C. Nayak, S. H. Simon, A. Stern, M. Freedman, and S. Das Sarma, Non-Abelian anyons and topological quantum computation, Rev. Mod. Phys. **80**, 1083 (2008).

[2] J. Alicea, Y. Oreg, G. Refael, F. von Oppen, and M. P. A. Fisher, Non-Abelian statistics and topological quantum information processing in 1D wire networks, Nat. Phys. **7**, 412 (2011).

[3] T. Hyart, B. van Heck, I. C. Fulga, M. Burrello, A. R. Akhmerov, and C. W. J. Beenakker, Flux-controlled quantum computation with Majorana fermions, Phys. Rev. B **88**, 035121 (2013).

[4] D. Aasen, M. Hell, R. V. Mishmash, A. Higginbotham, J. Danon, M. Leijnse, T. S. Jespersen, J. A. Folk, C. M. Marcus, K. Flensberg, and J. Alicea, Milestones Toward Majorana-Based Quantum Computing, Phys. Rev. X **6**, 031016 (2016).

[5] T. Karzig, C. Knapp, R. M. Lutchyn, P. Bonderson, M. B. Hastings, C. Nayak, J. Alicea, K. Flensberg, S. Plugge, Y. Oreg, C. M. Marcus, and M. H. Freedman, Scalable designs for quasiparticle-poisoning-protected topological quantum computation with Majorana zero modes, Phys. Rev. B **95**, 235305 (2017).

[6] A. Y. Kitaev, Unpaired Majorana fermions in quantum wires, Phys. Usp. **44**, 131 (2001).

[7] A. Y. Kitaev, Fault-tolerant quantum computation by anyons, Ann. Phys. **303**, 2 (2003).

[8] G. E. Volovik, Fermion zero modes on vortices in chiral superconductors, JETP Lett. **70**, 609 (1999).

[9] A. P. Mackenzie and Y. Maeno, The superconductivity of Sr_2RuO_4 and the physics of spin-triplet pairing, Rev. Mod. Phys. **75**, 657 (2003).

[10] M. Stone and R. Roy, Edge modes, edge currents, and gauge invariance in $p_x + ip_y$ superfluids and superconductors, Phys. Rev. B **69**, 184511 (2004).

[11] J. D. Sau, R. M. Lutchyn, S. Tewari, and S. Das Sarma, Generic New Platform for Topological Quantum Computation Using Semiconductor Heterostructures, Phys. Rev. Lett. **104**, 040502 (2010).

[12] R. M. Lutchyn, J. D. Sau, and S. Das Sarma, Majorana Fermions and a Topological Phase Transition in Semiconductor-Superconductor Heterostructures, Phys. Rev. Lett. **105**, 077001 (2010).

[13] Y. Oreg, G. Refael, and F. von Oppen, Helical Liquids and Majorana Bound States in Quantum Wires, Phys. Rev. Lett. **105**, 177002 (2010).

[14] T. D. Stanescu, R. M. Lutchyn, and S. Das Sarma, Majorana fermions in semiconductor nanowires, Phys. Rev. B **84**, 144522 (2011).

[15] R. M. Lutchyn, E. P. A. M. Bakkers, L. P. Kouwenhoven, P. Krogstrup, C. M. Marcus, and Y. Oreg, Majorana zero modes in superconductor-semiconductor heterostructures, Nat. Rev. Mater. **3**, 52 (2018).

[16] J. Alicea, Majorana fermions in a tunable semiconductor device, Phys. Rev. B **81**, 125318 (2010).

[17] V. Mourik, K. Zuo, S. M. Frolov, S. R. Plissard, E. P. A. M. Bakkers, and L. P. Kouwenhoven, Signatures of Majorana fermions in hybrid superconductor-semiconductor nanowire devices, Science **336**, 1003 (2012).

[18] M. T. Deng, C. L. Yu, G. Y. Huang, M. Larsson, P. Caroff, and H. Q. Xu, Anomalous zero-bias conductance peak in a Nb-InSb nanowire-Nb hybrid device, Nano Lett. **12**, 6414 (2012).

[19] M. T. Deng, S. Vaitiekenas, E. B. Hansen, J. Danon, M. Leijnse, K. Flensberg, J. Nygård, P. Krogstrup, and C. M. Marcus, Majorana bound state in a coupled quantum-dot hybrid-nanowire system, Science **354**, 1557 (2016).

[20] M. T. Deng, S. Vaitiekenas, E. Prada, P. San-Jose, J. Nygård, P. Krogstrup, R. Aguado, and C. M. Marcus, Nonlocality of Majorana modes in hybrid nanowires, Phys. Rev. B **98**, 085125 (2018).

[21] S. M. Cronenwett, T. H. Oosterkamp, and L. P. Kouwenhoven, A tunable Kondo effect in quantum dots, Science **281**, 540 (1998).

[22] D. Goldhaber-Gordon, H. Shtrikman, D. Mahalu, D. AbuschMagder, U. Meirav, and M. A. Kastner, Kondo effect in a single-electron transistor, Nature (London) **391**, 156 (1998).

[23] G. Kells, D. Meidan, and P. W. Brouwer, Near-zero-energy end states in topologically trivial spin-orbit coupled superconducting nanowires with a smooth confinement, Phys. Rev. B **86**, 100503(R) (2012).

[24] E. J. H. Lee, X. Jiang, M. Houzet, R. Aguado, C. M. Lieber, and S. De Franceschi, Spin-resolved Andreev levels and parity crossings in hybrid superconductor-semiconductor nanostructures, Nat. Nanotechnol. **9**, 79 (2014).

[25] C.-X. Liu, J. D. Sau, and S. Das Sarma, Distinguishing topological Majorana bound states from trivial Andreev bound states: Proposed tests through differential tunneling conductance spectroscopy, Phys. Rev. B **97**, 214502 (2018).

[26] M. Hell, K. Flensberg, and M. Leijnse, Distinguishing Majorana bound states from localized Andreev bound

states by interferometry, Phys. Rev. B **97**, 161401(R) (2018).

[27] Y.-H. Lai, J. D. Sau, and S. Das Sarma, Presence versus absence of end-to-end nonlocal conductance correlations in Majorana nanowires: Majorana bound states versus Andreev bound states, Phys. Rev. B **100**, 045302 (2019).

[28] T. D. Stanescu and S. Tewari, Robust low-energy Andreev bound states in semiconductor-superconductor structures: Importance of partial separation of component Majorana bound states, Phys. Rev. B **100**, 155429 (2019).

[29] A. Schuray, L. Weithofer, and P. Recher, Fano resonances in Majorana bound states–quantum dot hybrid systems, Phys. Rev. B **96**, 085417 (2017).

[30] E. Prada, R. Aguado, and P. San-Jose, Measuring Majorana nonlocality and spin structure with a quantum dot, Phys. Rev. B **96**, 085418 (2017).

[31] C. Moore, C. Zeng, T. D. Stanescu, and S. Tewari, Quantized zero-bias conductance plateau in semiconductor-superconductor heterostructures without topological Majorana zero modes, Phys. Rev. B **98**, 155314 (2018).

[32] J. E. Sanches, L. S. Ricco, Y. Marques, W. N. Mizobata, M. de Souza, I. A. Shelykh, and A. C. Seridonio, Majorana molecules and their spectral fingerprints, Phys. Rev. B **102**, 075128 (2020).

[33] D. E. Liu and H. U. Baranger, Detecting a Majorana-fermion zero mode using a quantum dot, Phys. Rev. B **84**, 201308(R) (2011).

[34] V. L. Campo, L. S. Ricco, and A. C. Seridonio, Isolating Majorana fermions with finite Kitaev nanowires and temperature: Universality of the zero-bias conductance, Phys. Rev. B **96**, 045135 (2017).

[35] L. S. Ricco, V. L. Campo, I. A. Shelykh, and A. C. Seridonio, Majorana oscillations modulated by Fano interference and degree of nonlocality in a topological superconducting-nanowire–quantum-dot system, Phys. Rev. B **98**, 075142 (2018).

[36] W. J. Gong, S. F. Zhang, Z. C. Li, G. Y. Yi, and Y. S. Zheng, Detection of a Majorana fermion zero mode by a T-shaped quantum-dot structure, Phys. Rev. B **89**, 245413 (2014).

[37] P. Majek, K. P. Wójcik, and I. Weymann, Spin-resolved thermal signatures of Majorana-Kondo interplay in double quantum dots, Phys. Rev. B **105**, 075418 (2022).

[38] D. Rainis and D. Loss, Majorana qubit decoherence by quasiparticle poisoning, Phys. Rev. B **85**, 174533 (2012).

[39] M. P. Anantram and S. Datta, Current fluctuations in mesoscopic systems with Andreev scattering, Phys. Rev. B **53**, 16390 (1996).

[40] B. Zocher and B. Rosenow, Modulation of Majorana-Induced Current Cross-Correlations by Quantum Dots, Phys. Rev. Lett. **111**, 036802 (2013).

[41] Y. Meir and N. S. Wingreen, Landauer Formula for the Current Through an Interacting Electron Region, Phys. Rev. Lett. **68**, 2512 (1992).

[42] A. P. Jauho, N. S. Wingreen, and Y. Meir, Time-dependent transport in interacting and noninteracting resonant-tunneling systems, Phys. Rev. B **50**, 5528 (1994).

[43] H. Song, Z. Zhang, D. Pan, D. Liu, Z. Wang, Z. Cao, L. Liu, L. Wen, D. Liao, R. Zhuo, D. E. Liu, R. Shang, J. Zhao, and H. Zhang, Large zero bias peaks and dips in a four-terminal thin InAs-Al nanowire device, Phys. Rev. Res. **4**, 033235 (2022).

[44] Z. Y. Zeng and F. Claro, Delocalization and conductance quantization in one-dimensional systems attached to leads, Phys. Rev. B **65**, 193405 (2002).

[45] Y. Zheng, T. Lü, C. Zhang, and W. Su, Antiresonance of electron tunneling through a quantum dot array, Physica E **24**, 290 (2004).

[46] Further description of the superconducting phase dependence of the zero-bias conductances in the cases of $N = 3$ and 4.